Journal of Non-Crystalline Solids 358 (2012) 2179–2182

Contents lists available at SciVerse ScienceDirect

Journal of Non-Crystalline Solids

journal homepage: www.elsevier.com/locate/jnoncrysol

EELS measurements of boron concentration profiles in p-a-Si and nip a-Si solar cells

Bas B. Van Aken [a,*], Martial Duchamp [b], Chris B. Boothroyd [b], Rafal E. Dunin-Borkowski [c], Wim J. Soppe [a]

[a] ECN Solar Energy, P.O. Box 1, NL-1755 ZG Petten, The Netherlands
[b] Centre for Electron Nanoscopy, Technical University of Denmark, DK-2800 Kongens Lyngby, Denmark
[c] Institute for Microstructure Research, Forschungszentrum Jülich, D-52425 Jülich, Germany

A R T I C L E I N F O

Article history:
Received 16 August 2011
Received in revised form 6 December 2011
Available online 12 January 2012

Keywords:
Electron energy loss spectroscopy (EELS);
Thin film Si;
Transmission electron microscopy;
p-Type SiC;
Doping concentration

A B S T R A C T

The p-type Si layer in a-Si and μc-Si solar cells on foil needs to fulfil several important requirements. The layer is necessary to create the electric field that separates the photo-generated charge carriers; the doping also increases the conductivity to conduct the photocurrent to the front contact; on the other hand, the p-layer should transmit the incident light efficiently to the intrinsic absorber layer. We show that it is possible to study TEM samples prepared, for analysis of possible layer defects, by focussed ion beam milling to detect boron and carbon concentrations as low as 10^{20} cm^{-3}, using core-loss EELS combined with numerical analysis. We control the band gap and activation energy of p-a-SiC by varying the B_2H_6 and CH_4 flow during deposition in the process chamber. We have found a linear relation between the activation energy of the dark conductivity E_{act} and the optical band gap E_{04}. Modelling shows that the optimum efficiency in nip solar cells is obtained when the p-a-SiC band gap is slightly larger than the band gap of the absorber layer. We have assessed the potential of core-loss EELS for detecting B and C concentrations as low as 10^{20} cm^{-3} in a spatially resolved manner, and of low-loss EELS as a probe of the local variations in plasmon energy.

© 2011 Elsevier B.V. All rights reserved.

1. Introduction

Roll-to-roll production of thin film Si solar cells has several advantages over batch-type reactor systems, for instance high-throughput fabrication and the opportunity to make lightweight and flexible products. Flexible and lightweight PV modules gear up to building integrated PV: the most important market for PV in densely populated, developed countries [1,2]. ECN is developing a concept for roll-to-roll production of high efficiency nip solar cells based on amorphous (a-Si:H) and microcrystalline (μc-Si:H) silicon thin films on steel foil coated with an insulating barrier layer and sputtered back contact and reflection layer.

The p-type Si layer in a-Si and μc-Si solar cells on foil has several important requirements. The layer is necessary to create the electric field that separates the photo-generated charge carriers; the doping also increases the conductivity to conduct the photocurrent to the front contact; on the other hand, the p-layer should transmit the incident light efficiently to the intrinsic absorber layer. To obtain good conductivity, the typically required B concentration is ~10^{21} cm^{-3} in the thin p-a-Si layer, or about 2% [3]. Diffusion of dopants should be avoided, since the adjacent intrinsic absorber layer should have impurity concentrations below 10^{17} cm^{-3} [3]. To increase the amount of transmitted light through the p-doped Si layer, this layer is typically alloyed with C (referred to as p-a-SiC).

To make high efficiency Si solar cells, it is very important to control and limit the diffusion of B and C atoms into the i-layer during the consecutive processing of the solar cells. SIMS profiles have been realised on flat solar cells. These solar cells show an improved efficiency when the B contamination is low in the i-layer. However, the i/p interface has an average roughness of ~10 nm, which is about the thickness of the p-layer. This makes an accurate determination of the B depth profile at the i/p interface with SIMS impractical as the probe diameter is of the order of 1 μm. In such cases, electron energy loss spectroscopy (EELS) in the transmission electron microscope (TEM) may combine the necessary spatial resolution (down to 1 nm) with sufficient sensitivity to the boron content and the carrier concentration to investigate the boundary between p-a-SiC and i-a-Si.

2. Experimental procedures

All TEM samples used in this study consist of Ag/ZnO back contacts and ITO window layers, both sputtered in an AJA sputter tool. The silicon deposition is carried out in the Flexicoat300, an industrial pilot roll-to-roll system for PECVD of doped and intrinsic silicon layers suitable for foils of width up to 300 mm. The Flexicoat300 has three inline deposition chambers. Two chambers are equipped with the previously reported linear symmetric RF (13.56 MHz) sources [4,5], which are excellently suited for deposition of amorphous and microcrystalline doped silicon layers. The intrinsic Si absorber layers are deposited with a linear VHF plasma source (70 MHz). Samples (typically substrates of 10×2.5 cm^2) are fixed to a custom-made sample holder, which is placed in the steel foil that in these experiments

* Corresponding author. Tel.: +31 224 564905; fax: +31 224 568214.
E-mail address: vanaken@ecn.nl (B.B. Van Aken).

0022-3093/$ – see front matter © 2011 Elsevier B.V. All rights reserved.
doi:10.1016/j.jnoncrysol.2011.12.055

functions as conveyor belt. The vacuum chambers are separated by independently pumped gas sluices to prevent (cross-)contamination. The main advantages of linear plasma sources are that deposition uniformity is only required in one direction, perpendicular to the motion of the substrate(s) and the ease of upscaling the plasma sources to enable deposition on foil substrates of one metre width or more.

Single layers are deposited on Corning2000 glass in the p-type RF chamber of the Flexicoat300. These samples were analysed for electrical and optical properties. For conductivity measurements Al contacts are evaporated by e-beam. The activation energy and dark conductivity is measured with a 2-point set-up using a Keithley-595 quasistatic C-V metre, in a cooling-down run from 393 K to room temperature under vacuum. A single beam photospectrometer has been used to measure the transmittance and reflectance. This set-up was equipped with an integrating sphere to handle the effect of rough or porous layers.

Thin film silicon solar cells consist of a plastic, glass or metallic substrate, several metal and oxide layers and the active Si solar cell itself. Due to the different milling rates of the constituting layers, sample fabrication for TEM is relatively difficult. Also, during exposure, care has to be taken not to damage the sample area of interest. Nevertheless, we succeeded in preparing 100 nm thick and 5 μm wide TEM lamellae by focussed ion beam (FIB), where the final milling step has been made with a 5 keV Ga^{2+} beam. A bright-field (BF) TEM image of the a-Si solar cell sample is shown in Fig. 1a. In order to enhance the contrast from the SiC region, a so-called *thickness-over-lambda* (d/λ) map is shown in Fig. 1b. The p-layer appears dark compared to ITO and Si due to the larger mean free path λ of inelastic electron scattering of SiC compared to Si.

EELS-TEM is a spectrometric technique which allows measuring the energy loss of an electron beam when travelling through the TEM specimen. Fig. 2 shows a typical EELS spectrum, indicating the plasmon loss region and the core-loss region. The physical processes involved in energy-loss can be (i) band gap transition, (ii) plasmon collective oscillation and (iii) interatomic transition. Therefore, they can provide information on (a) the band gap energy, (b) the carrier density (through the plasmon energy) and (c) the local atomic composition with a nanometre range spatial resolution [6].

EELS has been performed on a FEI Tecnai T-20 equipped with a LaB6 electron source and, when higher spatial resolution was needed, on a FEI Titan 80-300 equipped with a field emission electron source and a Gatan Tridiem imaging filter. Spectra were acquired in TEM-diffraction mode. All data taking was carried out at 120 keV to limit damage of the sample by the electron beam.

The core-loss EELS data have been averaged and background subtracted to isolate the B peak. For each area, six EELS spectra shifted in energy were acquired. Channel to channel gain variations were reduced using the iterative averaging process described in detail elsewhere [7]. To minimise the shot noise, the exposure time was kept as high as possible without damaging the specimen. For the large area measurements, each spectrum was acquired for 1 min with a beam diameter of about 200 nm. For higher spatial resolution, line

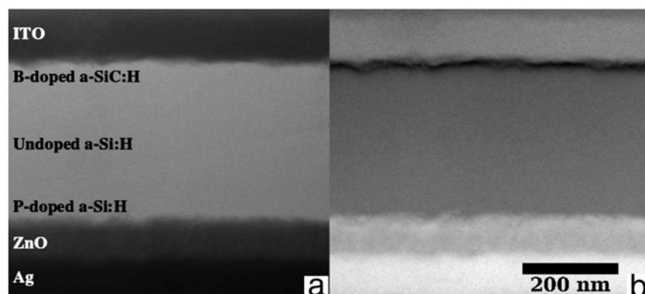

Fig. 1. TEM images in (a) bright field and (b) d/λ map of an a-Si solar cell prepared by FIB milling.

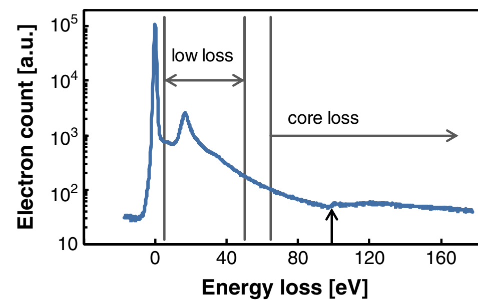

Fig. 2. Example of an EELS spectrum, showing the zero-loss peak, the low-loss region due to plasmon absorption and the core-loss region. The ionisation energy of Si, at 99 eV, is also indicated.

scans were made with a 5 nm beam in TEM diffraction mode. Each spectrum was acquired for 1.5 s. Details of the method are given elsewhere [8].

The low-loss EELS data have been acquired in scanning TEM. To accurately determine the absolute value of the plasmon energy, we have fitted both the zero loss peak and the bulk plasmon peak to an appropriate function using the least squares method, leading to errors of 0.067% and 0.016%, respectively. The absolute plasmon energy was taken as the difference between the fitted peak positions in eV of the bulk plasmon peak and the zero loss peak. According to theory, the bulk plasmon energy E_p increases with the square root of the valence electron density.

3. Results

The electrical and optical properties of p-a-SiC are mainly determined by the amounts of (active) B and C present in the layer. In our case, B increases the conductivity of a-Si up to $\sigma_d > 10^{-3}$ S/cm but also increases the absorption of photons by decreasing the E_{04} to ~1.6 eV. In contrast, alloying intrinsic a-Si with C increases the E_{04} to ~2.4 eV and decreases the σ_d far below 10^{-10} S/cm.

We varied the flow rates of B_2H_6 and CH_4, whilst keeping the other process conditions constant for a series of samples. An increase of CH_4 has the same effect as a decrease of B_2H_6, i.e. the dark conductivity increases, but the band gap becomes lower. Fig. 3 shows the measured E_{04} and E_{act} of these samples; the ratio CH_4:SiH_4 varied between 0.2 and 2.0 and the ratio B_2H_6:SiH_4 between 0.3 and 3.2%. The data point of C-free p-a-Si would be in the left corner at E_{act} <0.3 eV and E_{04}~1.6 eV. For this set of p-a-SiC samples, we have found evidence for a linear correlation between the E_{act} and the E_{04}. This means that only a single line in (E_{act}, E_{04}) space is accessible. Although, the two elements B and C have opposite effects, they don't cancel each other completely. The combination of good dark conductivity and high band gap is obtained at low amounts of addition to the a-Si deposition

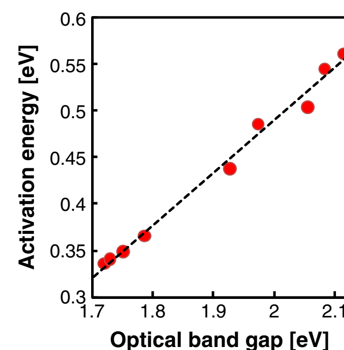

Fig. 3. The activation energy of dark conductivity as a function of the optical band gap E_{04} for the series of p-a-SiC samples, with a variation in B and C concentrations. The dashed line is a linear fit to the data.

process. To determine the optimal, but also accessible, properties of the p-a-SiC window layer, we have to resort to modelling, as simple deduction (high optical band gap and low activation energy) is not sufficient.

We have modelled a series of solar cells with ASA [9] to resolve the competition between transmission (high band gap) and conductivity (low activation energy). We varied the p-a-SiC by changing the E_{04} for constant values of E_{act} and plotted the obtained efficiency η in Fig. 4. With increasing E_{act}, the η is subsequently lower for all values of E_{04}. At constant E_{act}, the η increases with increasing E_{04}, except for high values of E_{act} when the efficiency starts to drop, even though the band gap is increasing. Particularly, the efficiency η falls strongly for $E_{act} > 0.5$ eV. Looking at the underlying JV-graphs, the drop in E_{act} is mainly due to a deteriorating fill factor.

Looking at the experimentally obtained data points, indicated in Fig. 4 by the dashed line, the optimum efficiency is found for a p-layer with an optical band gap of ~1.9 eV, a value just above that of the intrinsic layer. The activation energy is for that point just lower than 0.5 eV, in good agreement with published device quality values [10]. At even higher band gap p-layers, the increase in transmission is more than offset by the deteriorating fill factor, whereas at lower band gap the absorption in the p-layer increases, thus the generation of charge carriers in the i-layer is reduced.

We studied the B and C concentration profiles using core-loss EELS TEM. Experimental and calculated background subtracted B K-edge EELS spectra measured on the SiC test sample containing different B concentrations are shown in Fig. 5. The B peak of the highly doped sample is clearly recognisable and fits well with the simulated B peak after adjusting for the crystallinity and the cluster size. The composition has been estimated using the Hartree–Fock cross-sections, with $\sigma_{Si} = 14{,}111 \pm 1411$ b and $\sigma_B = 5240 \pm 524$ b, so the relative error on the absolute boron concentration is ~20%. However, for concentration profiles (see Fig. 6) the errors on the cross-sections are constant, thus the determination of the B profile, that is the variation of the Si/B ratio, is much more accurate. As the B peak is quite narrow, we used an 8 eV integration window to calculate the area below the curves. For the intrinsic layer, no significant B concentration was measured by EELS. The B concentration of the p^+-a-SiC is 0.6 ± 0.1 at.%, whereas the p^{++}-a-SiC has 2.0 ± 0.4 at.%. For comparison, SIMS measurements on the same sample yielded 0.6 and 3.0 at.%, respectively.

Fig. 6 shows the B concentration in a nip a-Si solar cell close to the ITO interface, measured with SIMS and with EELS applying a 5 nm beam diameter, that is about half the p-layer thickness. A slightly higher B concentration has been measured by EELS when compared to the SIMS profiles. The SIMS data is intrinsically the average over a relatively large area due to the size of the ion beam. This gives rises to slightly lower B concentration values and also slightly wider peaks. The carbon concentration as determined with SIMS is 16 at.%.

Fig. 6 is the proof of principle for determining the B concentration profile with EELS in the electron microscope on a sample with smooth interfaces. The main advantages of EELS are shown when microscopic details about the B concentration profile at the TCO/p or p/i interface are obtained by decreasing the beam diameter on a sample with rough interfaces (textured substrate).

We have used low-loss EELS to measure changes in plasmon energy and assess whether these changes are associated with active dopant concentration variations. The plasmon energy has been determined by the method described in the Experimental procedures section. The test sample consisted of a stack of three ~200 nm SiC layers with no (i-SiC), standard (p^+-SiC) and double (p^{++}-SiC) amounts of B doping sandwiched between standard back (ZnO/Ag) and front (ITO) contact layers. In Fig. 7, the plasmon energy (open symbols) has been plotted as a function of depth. For comparison the SIMS profile of the B concentration is shown as solid line. To estimate the relative B concentration obtained by SIMS, we assume that the total density of atoms is 5×10^{22} cm^{-3}, and typical error estimation for determining B in Si is ~10 at.% [11]. We clearly observe a strong relation between B concentration and plasmon energy. By assuming that the density of atoms and the carrier mobility are independent of the B-doping level, we can consider that the increase of B concentration increases the valence electron density. Furthermore, the TCO front and back contacts as well as the Ag layer can also be identified by unique levels of the plasmon energy at the expected depths (not shown in the graph).

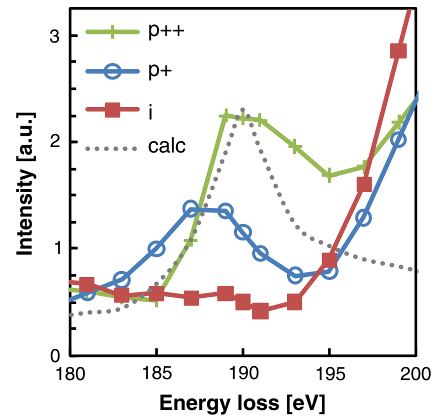

Fig. 5. Background subtracted core-loss EELS spectra of each of the three layers of the SiC stack. The dashed line shows the calculated profile of the boron core-loss peak. The error on these spectra is expected to be <0.01%, as the shot noise at the boron edge is ~0.003% and the noise from the CCD camera is ~0.005% after the iterative process [7].

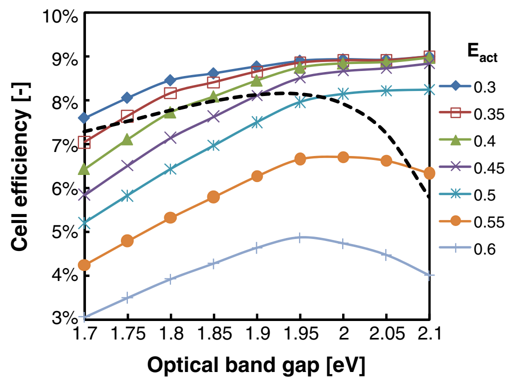

Fig. 4. Calculated efficiency of a-Si solar cells as a function of the optical band gap E_{04} of the p-a-SiC layer for seven values of the activation energy E_{act}, see legend. The efficiencies for solar cells with E_{04} and E_{act} of the p-a-SiC layer on the experimentally obtained relationship (see Fig. 3) are given by the dashed line.

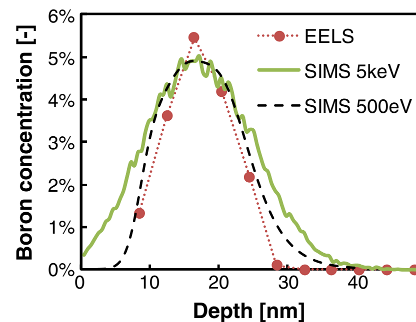

Fig. 6. Boron profiles determined by EELS (markers) and SIMS (lines). EELS data have been collected with a 5 nm probe beam. SIMS data have been measured at two different ion energies.

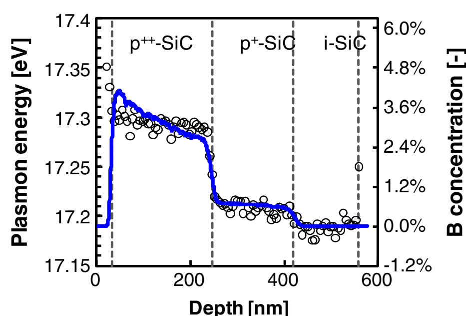

Fig. 7. Plasmon energy (open circles) as a function of depth in the triple SiC stack. The plasmon energy is determined from the low-loss EELS spectra, errors in energy (14 meV) and depth (2.5 nm) are smaller than symbols. The dashed lines indicate the locations of the interfaces. The B concentration profile (blue solid line) is shown on the right axis as determined by SIMS (data is averaged over 5 nm).

4. Conclusion

The optical band gap E_{04} and the activation energy E_{act} of p-a-SiC has been controlled by varying the diborane and methane flows in the deposition chamber. We have found a linear relationship between the experimentally observed combinations of E_{04} and E_{act}. Modelling of a-Si solar cells with these p-a-SiC layers shows that the highest efficiency is calculated for a p-layer with high E_{04} and low E_{act}. Restricting the data to points on the experimentally observed curve, we find that with increasing E_{04} and E_{act}, the efficiency slowly increases, until above $E_{04}=2.0$ eV and $E_{act}=0.50$ eV the maximum power drops dramatically.

The potential of core-loss EELS for detecting B and C concentrations as low as 10^{20} cm^{-3} is assessed, both in dedicated test samples and in "real" solar cells. As proof of concept, the B-concentration profile was measured with a 5 nm probe beam on a 200 nm thick p-Si layer and compared with the SIMS profile. The absolute concentration, as determined by EELS, is in reasonable agreement with the SIMS results. We also applied the EELS-TEM technique to a functioning a-Si solar cell. Again, the absolute concentrations are in good agreement. Since the concentration is not averaged across the lateral dimensions, as is the case with SIMS, EELS-TEM allows us to measure the B concentration profile of thin layers on rough interfaces, for instance when textured substrates have been applied.

Finally, low-loss EELS has been applied to study the plasmon energy as a function of the dopant level. The experimentally derived plasmon energy correlates well with the changes in B concentration in p-a-SiC and also shows sharp transitions at the TCO/Si interfaces. Low-loss EELS is thus an independent tool to study modifications of the band structure at very high resolution, which is particularly useful for rough interfaces and textured substrates.

To conclude, we have shown that high resolution TEM measurements yield valuable information on doping level and band structure of thin film Si solar cells. Future work will concern thin-film microcrystalline silicon solar cells where the electrical properties and the chemical composition of growth defects are open questions.

Acknowledgements

This work has been financially supported by the European Commission (Silicon-Light project, EU FP-7 Energy 2009-241477).

References

[1] M. Izu, T. Ellison, Sol. Energ. Mat. Sol. Cells 78 (2003) 613.
[2] A. Takano, T. Kamoshita, Jpn. J. Appl. Phys. 43 (2004) 7976.
[3] U. Krol, et al., Thin Solid Films 451 (2004) 525.
[4] B.B. Van Aken, et al., J. Non-Cryst. Solids 354 (2008) 2392.
[5] B.B. Van Aken, et al., SPIE Conf. Proc.: Photovoltaic Cell and Module Technologies, 6651, 2007, p. 0C-8.
[6] R.W. Kelsall, I.W. Hamley, M. Geoghegan, Nanoscale Science and Technology, John Wiley & Sons, Ltd., Chichester, UK, 2005.
[7] C.B. Boothroyd, K. Sato, K. Yamada, Proc. XIIth Int. Congress for Electron Microscopy, 1990, p. 80.
[8] M. Duchamp, et al., J. Phys. Conf. Series 326 (2011) 012052.
[9] M. Zeman, et al., Software Package: Amorphous Semiconductor Analysis (ASA), Delft University of Technology, The Netherlands, 2005.
[10] R.E.I. Schropp, M. Zeman, Amorphous and Microcrystalline Silicon Solar Cells — Modelling, Materials and Device Technology, Kluwer Academic Publishers, Dordrecht, the Netherlands, 1998.
[11] G. Stingeder, Anal. Chim. Acta 297 (1994) 231.